

# Fluid Structure Interaction Applied to Upper Aorta Blood Flow.

J.J. Anza<sup>1</sup>, M.A Esteves<sup>1</sup>

<sup>1</sup>Department of Applied Mathematics, University of the Basque Country, Spain

\*Corresponding author: Alameda de Urkijo s/n, 48013 Bilbao, Spain; juanjose.anza@ehu.es

**Abstract:** This work deals with the computer simulation of the blood flow, the arterial wall deformation and their 3D bidirectional interaction, including initial stresses and root displacements. The flow is laminar and steady with flexible walls modeled with a hyperelastic Demiray material model. Poiseuille formula is used to check the bidirectional interaction. 2D axisymmetric and full 3D models have been used and some considerations are made to the weak contribution of the boundary load interface. Initial stresses consider the fact that geometric dimensions corresponds to in vivo measured arteries, normally under diastolic pressure. Cylindrical components have to be converted to Cartesian at each point, being necessary to generate new variables to add to the regular hyperelastic stress components. This way of deformations are realistic and not extremely large. Finally, upper aorta is modeled as a torus with 3 cylinders (ramifications) and reasonable results are obtained.

**Keywords:** Fluid Structure Interaction, Blood Flow, Upper Aorta, Initial Stresses, Hyperelastic Material.

## 1. Introduction

It is well known that cardiovascular function is characterized by, among other factors, a number of biomechanical indices and parameters such as the wall shear stress, that may be useful in the early characterization of degenerative arterial disease. Likewise, some clinical studies highlight the need for new hemodynamic indices which can come from an accurate interpretation of the biomechanics. Basic research is needed in order to improve our understanding of blood flow and the response of the arterial tissue. Experimental techniques, mathematical models and computer simulations, imaging and image analysis methods should provide a deeper understanding to be translated to clinical applications for the analysis, treatment or the prevention of diseases.

Mechanical factors may be important in triggering the onset of aneurysms or atherosclerosis, the major cause of human mortality in the western world. An efficient constitutive description of arterial walls can

improve diagnostics and therapeutic procedures, but blood velocity and pressure fields are influenced by the deformability of the vessel.

This work deals with computer simulation of the blood flow, the arterial wall deformation and their 3D bidirectional interaction, including initial stresses and root displacements.

## 2. Governing equations

We assume that the blood is incompressible and Newtonian; the flow is laminar and steady, with flexible walls. Four PDEs (Navier Stokes and incompressibility) are the conditions that allow solving for the 4 fluid unknowns: the 3 components of the fluid velocity and pressure, giving the pressure acting on the fluid-solid interface.

We assume that the arterial walls are elastic but nonlinear, governed by the three equilibrium equations and one constitutive equation relating the pressure with volumetric deformation. Four PDE allow solving for the 3 solid displacements components, and for the hydrostatic part of stress that is independently approximated to consider the solid to be nearly incompressible avoiding mesh locking.

The integration of the weak form of the equilibrium equations is done on the initial undeformed domain  $V$ , using Piola II ( $\mathbf{S}$ ) as stress measure and Green ( $\mathbf{E}$ ) as deformation measure

$$\int_V \mathbf{S} : \delta \mathbf{E} dV = \int_V \mathbf{t} \frac{da}{dA} \cdot \delta \mathbf{u} dA + \int_V J \mathbf{f} \cdot \delta \mathbf{u} dV$$

where  $J$  is the volume ratio, and  $\delta \mathbf{E}$  and  $\delta \mathbf{u}$  are the test functions (virtual displacements).

Piola stress  $\mathbf{S}$  is obtained from a hyperelastic energy potential, composed of an isochoric and a volumetric part:

$$W = W_{iso} + W_{vol}$$

For the isochoric part we have used a Demiray material type:

$$W_{iso} = \frac{a}{b} \left[ \exp \left( \frac{b}{2} (I_1 - 3) - 1 \right) \right]$$

Where  $I_1$  is the first invariant of the deformation and  $a$  and  $b$  are material constants:  $a$  is the

initial elastic modulus and  $b$  shapes the traction curve, as is shown in fig 1.

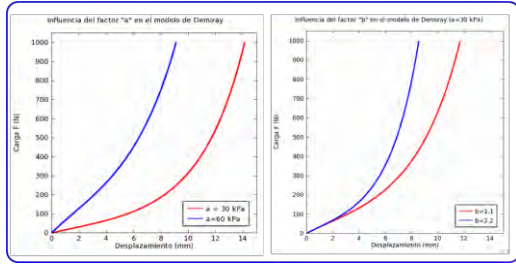


**Figure 1.** Traction curves for  $\{a=30, 60 \text{ Kpa}, \text{ with } b=1\}$ ; and  $\{b=1.1, 2.2 \text{ with } a=30\text{Kpa}\}$ .

The isochoric potential is supplemented with a very stiff volumetric expression allowing quasi-incompressibility:

$$W_{vol} = \frac{1}{2}k(J^2 - 1) \quad ; \quad k \approx \frac{10000}{3} \cdot a$$

Three Laplace PDE govern the movement of the fluid mesh, being Dirichlet boundary conditions the solid displacements at the interface.

After discretization with  $n$  non Dirichlet nodes we will have to solve a nonlinear problem with  $11 \times n$  coupled unknowns. This can be done in a full coupled way or in a segregated one dividing the unknowns by groups being the second method more convenient for large meshes.

When using the segregated method we have organized the unknowns in the 3 physical groups that are solved iteratively in this order: mesh-fluid-solid. Linear systems for the fluid unknowns are solved by iterative methods and directly for the solid and the mesh unknowns.

### 3. Use of COMSOL Multiphysics

Comsol Model Library offers one example of one way 3D aorta interaction. In this study full bidirectional interaction is done, but some changes to the FSI interface have to be incorporate to obtain correct results. Initial stresses are also included in order to consider the fact that geometric dimensions corresponds to in vivo measured arteries, normally under diastolic pressure.

#### 3.1 Validation on a cylinder. Poiseuille flow adaptation to the deformation.

Poiseuille analytical formula for the viscous laminar flow in a circular pipe:

$$v = v_{max} \left( 1 - \frac{r^2}{R^2} \right) \quad , \quad v_{max} = \frac{GR^2}{4\eta}$$

Where  $G$  is the pressure drop per unit length,  $R$  is the radius and  $\eta$  the dynamic viscosity, is a good way to check the bidirectional interaction: the fluid pressure increases the pipe diameter in one way, and vice versa the flow velocity adapts to the deformation. With this aim we have go through the following steps:

#### 3.1.1 Laminar flow interface

Both 2D axisymmetric and full 3D models can be used for this problem. Figures 1 and 2 show similar results adjusting well to the parabolic velocity profile. Results have been obtained for a pressure outlet condition of 100 mmHg (13332 Pa) and an inflow inlet condition incremented in 2 Pa/cm. Viscosity is 0.005 Pa.s, density 960 kg/m<sup>3</sup> and the radius is 2 cm. P2 + P1 rectangles and hexahedral have been used with streamline stabilization.

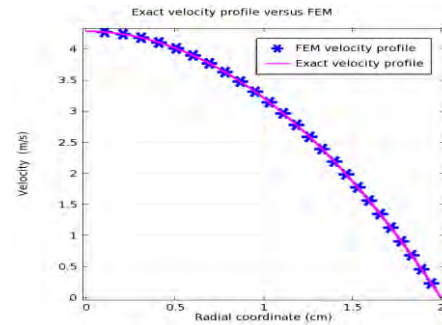


**Figure 2.** Velocity profile for axisymmetric model. Analytical and numerical results with rectangular elements.

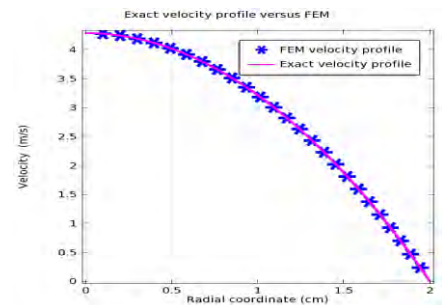


**Figure 3.** Velocity profile for 3D model. Analytical and numerical results with hexahedral elements.

#### 3.1.2. - Structural mechanics interface: cylinder under internal pressure

Wall thickness is 2 mm and Demiray material is used with  $a=1e5 \text{ Pa}$  and  $b=0.844$  (ref3) corresponding to experimental data for a

young male. Rollers are used as boundary conditions for the two extremes of the cylinder, and zero displacements are applied on lines of symmetry to avoid rigid movements.

Weak contribution of the pressure boundary load is done in the material frame and the ratio  $da/dA$  of the integral is considered with the ratio  $dvol\_spatial/dvol$  in the weak expression. Figs 3 and 4 show similar deformations computed in the 2D axisymmetric model and the full 3D with a maximum displacement (opening) of 3.34 mm ( $a=3e5$  Pa, rectangle and hexahedral quadratic elements.).

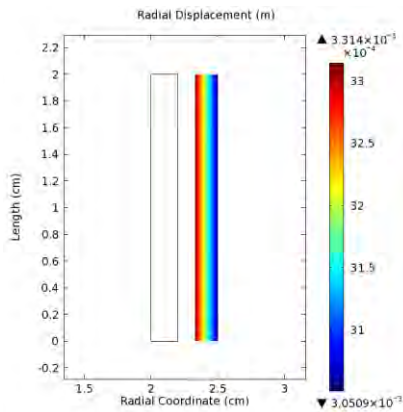


Figure 3. Axisymmetric model deformation.

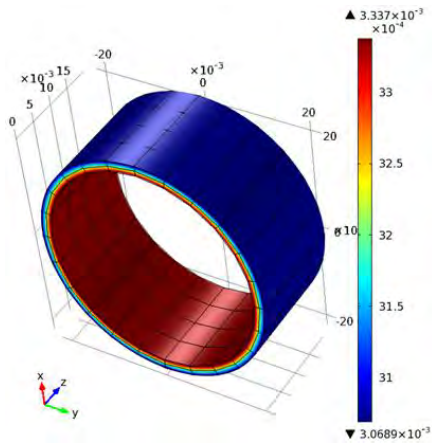


Figure 4. 3D model deformation.

### 3.1.3 FSI interface.

This interface contains the needed tools from the laminar interface and the structural mechanics as well as from the deformed mesh interface that couples both previous modes. With previous data the 2D axisymmetric ale problem gives the same deformation: 3.34 mm for the maximum radial displacement but the 3D ale model gives 4.28 mm.

The FSI interface integrates the domain fluid weak expression in the spatial frame as the laminar flow interface, the domain solid weak expression in the material frame as the structural mechanics interface, and the weak contribution of fluid-solid interface boundary load, given by the fluid, in the spatial frame, but retaining the factor  $dvol\_spatial/dvol$  as in the weak contribution of the pressure boundary load of the structural mechanics interface. In our opinion this factor should be removed now, at least for this problem, and indeed, once removed 3.34 mm are again obtained for the maximum radial displacement.

$$\int_{\partial V} \mathbf{t} \delta \mathbf{u} \, da = \int_{\partial V} \mathbf{t} \frac{da}{dA} \delta \mathbf{u} \, dA \quad \left\{ \begin{array}{l} \partial V : \text{deformed domain boundary} \\ \partial V : \text{undeformed dom. bound.} \end{array} \right.$$

Now the full interaction works well and the computed velocity adapts properly to the theoretical Poiseuille profile with the deformed diameter, as fig 6 shows:

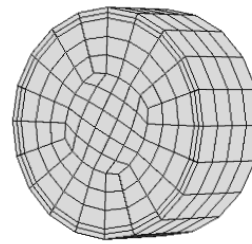


Figure 5. Mesh for the fluid and the solid.

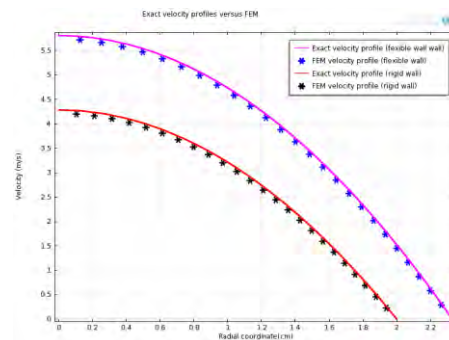


Figure 6. Velocity profiles before and after deformation, Analytical and numerical results.

Convergence is achieved in an incremental way, starting with a very stiff material  $a \rightarrow 100a$ , and advancing through the sequence  $\{100, 10, 8, 6, 4, 3, 2, 1\}$ . Anyway, pressure results degrade after  $3a$  because inflow inlet condition works poorly for openings greater than 3.34 mm (in this problem). Switching than to a pressure condition for the inlet (specified as outlet-pressure) you have correct pressure but you lose precision in the maximum velocity of

the parabolic profile. This is a fluid problem that also happens with rigid walls and it can be improved with finer hexahedral meshes and using P1+P1 discretization without stabilization or finer tetrahedral meshes using P2+P1 with streamline stabilization.

### 3.2 Initial stress:

Realistic aorta geometries are constructed from medical images obtained with angiographic methods or TACs in vivo, normally under diastolic internal pressure. It is then necessary to consider as initial stresses the existing stress in equilibrium with the geometry. This way stress increments from diastole to systole are correctly considered, not overestimating deformation increments as can be seen in fig.7.

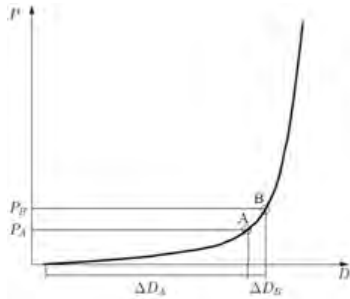


Figure 7. Traction curve for an arterial tissue showing the characteristic stiffening with deformation

Initial stresses is a solid feature that is handled in the structural mechanics interface. Elastic material implements a specific section to define initial stresses in Cartesian coordinate, but hyperelastic material does not, and it is necessary to define new variables for the initial stress components and add them up to the regular stress variables deduced from the strain energy potential. All this has been done in the structural mechanics interface.

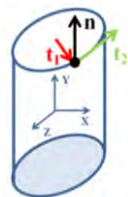
In our problem, initial stresses have been estimated with the thin wall formulas for the cylinder under internal pressure.

#### 3.2.1 Cylinder: 2D axisymmetric and full 3D models.

Initial stresses in cylindrical coordinates have been considered as follows (longitudinal cylindrical axis coincides with Cartesian y axis).

$$\bar{\sigma} = \begin{Bmatrix} 0 & 0 & 0 \\ 0 & pr/e & 0 \\ 0 & 0 & 0 \end{Bmatrix}$$

$$r = \sqrt{x^2 + z^2}$$



Boundary conditions for the 2 extremes of the cylinder are rollers, and only circumferential stress component has been considered. This stress tensor is valid for the axisymmetric model, but it has to be converted to Cartesian components for the 3D model in the following way:

$$t_1 = \frac{1}{r} \begin{Bmatrix} x \\ 0 \\ z \end{Bmatrix} ; n = \begin{Bmatrix} 0 \\ 1 \\ 0 \end{Bmatrix} ; t_2 = n \times t_1 = \frac{1}{r} \begin{Bmatrix} z \\ 0 \\ -x \end{Bmatrix}$$

$$Q^T = \begin{Bmatrix} t_1 \\ t_2 \\ n \end{Bmatrix} ; \sigma = Q \bar{\sigma} Q^T = \frac{pr}{e} \begin{Bmatrix} z^2 & 0 & -zx \\ 0 & 0 & 0 \\ -xz & 0 & x^2 \end{Bmatrix}$$

Fig 8 shows the results obtained for the axisymmetric model. Internal pressure of 80 mmHg has been considered, with Demiray material (a = 1e5 Pa, b = 0.844).

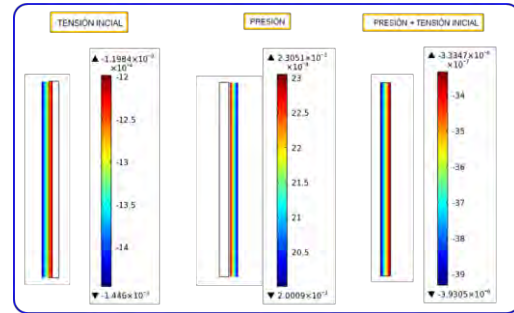


Figure 8. Only initial stress, only internal pressure, both simultaneously.

Fig 9 compares the results obtained for 120 mmHg internal (systolic) pressure, without and considering initial stresses for 80 mmHg.

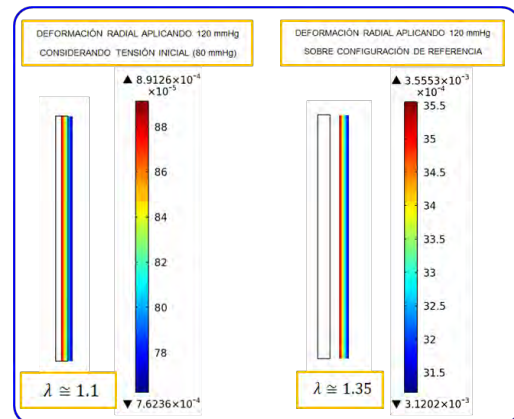


Figure 9. Considering initial stresses and not considering.

Similar results are obtained for the full 3D model.

### 3.2.2 Torus:

The torus geometry is one step further towards the upper aorta geometry. The major radius is  $\hat{R} = 3.9$  cm, the minor 2 cm and the thickness  $e = 2$  mm. As in the cylinder case, the median longitudinal plane of the torus is the  $xy$  plane of symmetry. Boundary conditions for the two extreme of the torus are rollers and zero displacements are applied on lines of symmetry to avoid rigid movements.

Longitudinal initial stresses are now considered, together with the circumferential ones. As before, cylindrical components are transformed to Cartesian. Given a point  $(x, y, z)$ ,  $\rho$  is the projection on the  $xy$  plane of the distance to the origin (center of the torus) and  $r$  is de distance from the point to center of the plane section that contains the point. Then:

$$\rho = \sqrt{x^2 + y^2} \quad ; \quad r = \sqrt{(\rho - \hat{R})^2 + z^2}$$

$$t_1 = \frac{1}{r} \begin{bmatrix} (\rho - \hat{R}) \frac{x}{\rho} \\ (\rho - \hat{R}) \frac{y}{\rho} \\ z \end{bmatrix} \quad ; \quad n = \frac{1}{\rho} \begin{bmatrix} y \\ -x \\ 0 \end{bmatrix} \quad ; \quad t_2 = n \times t_1$$

$$Q^T = \begin{bmatrix} t_1 \\ t_2 \\ n \end{bmatrix} \quad ; \quad \bar{\sigma} = \frac{1}{e} \begin{bmatrix} 0 & 0 & 0 \\ 0 & pr & 0 \\ 0 & 0 & pr/2 \end{bmatrix} \quad ; \quad \sigma = Q \bar{\sigma} Q^T$$

Fig 10 shows the expansion of the torus when only subjected to internal pressure of 100 mmHg. Fig 11 shows the contraction when the torus is only subjected to corresponding initial stresses. When both are together consider, the effects compensate and final deformation is practically null.

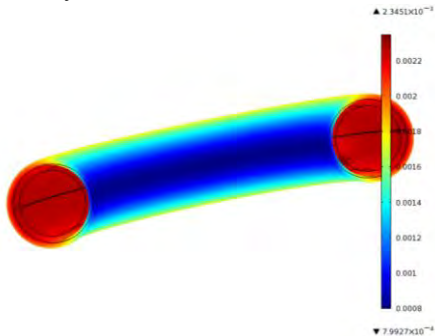


**Figure 10.** Expansion of the torus under internal pressure.

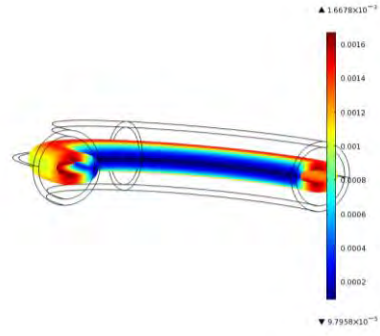


**Figure 11.** Contraction of the torus with only initial stresses. Magnification factor is 5.

Finally the whole picture including fluid flow and initial stresses has been studied with the FSI interface.

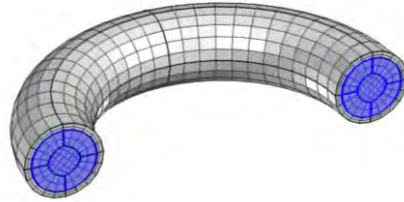


**Figure 12.** Mesh for the fluid and the solid.

Now symmetry respect the central section of the torus is lost, due to the action of the fluid, and the inlet section has to be fixed to avoid rigid movements. Fluid and solid data are the same as previous cases but now  $a = 1e5$  Pa can be considered, because inlet section does not deform and does not limit the correct behavior of the pressure inflow inlet condition.

Fig 13 and 14 show the influence of using or not initial stresses. The fluid outlet pressure corresponds to 120 mmHg (systole) but the geometry and initial stresses correspond to 80 mmHg (diastole).

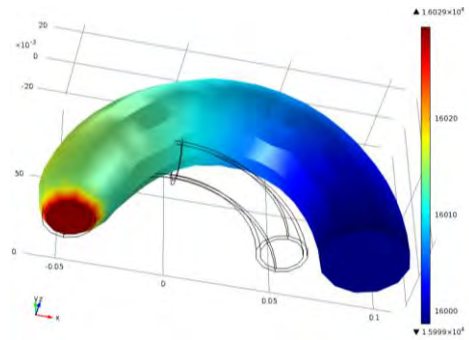


**Figure 13.** Pressure and deformation at the fluid-solid interface for 120 mmHg without initial stress.

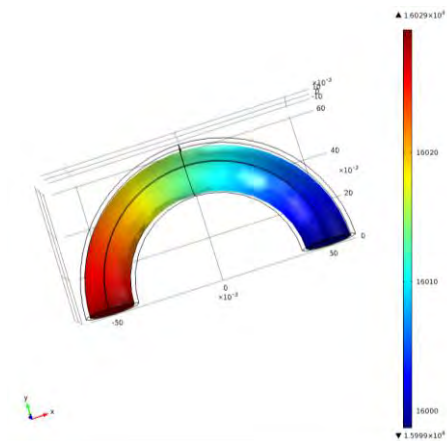


**Figure 14.** Pressure and deformation at the fluid-solid interface, for 120 mmHg with initial stresses corresponding to 120 mmHg.

Pressure precision deteriorates when using inflow inlet boundary condition with curved pipes. This can be arranged switching to pure pressure inlet condition (specified as outlet-pressure) but velocity results can be more instable.

### 3.2.3 Torus with 3 ramifications

This case is a combination of previous ones. Ramifications are modeled as vertical cylinders whose initial stresses have already been described. Nevertheless 4 hyperelastic materials have to be implemented in order to declare the needed additional variables for initial stresses computations: one for the torus and one for each ramification. The 3 are vertical but in different  $x$  position. It works as can be seen in next figures.

### 4. - Upper aorta results.

Upper aorta is modeled using the previous torus and 3 vertical ramifications.

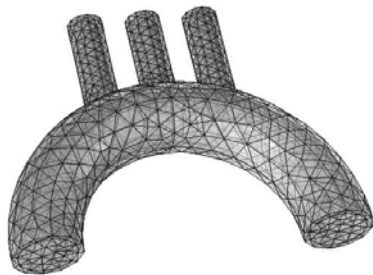


**Figure 15.** Mesh for the fluid and the solid.

Geometry, fluid and solid data as given in previous cases. Boundary conditions for outlet sections of the ramifications are rollers. Initial stresses are considered in all cases.

Fig 16 corresponds to 80 mmHg geometry, initial stresses and internal pressure. Inlet pressure is 10700 Pa and outlet pressures are respectively: 10681, 10677, 10673 and 10670.



**Figure 16.** Fluid velocity and solid deformation

Fig 17 corresponds to 80 mmHg geometry and initial stresses, and 120 mmHg internal pressure. Inlet pressure is 16030 Pa and outlet pressures are respectively: 16011, 16007, 16003 and 16000.



**Figure 17.** Fluid velocity and solid deformation

Finally we have modelled with the fluid-solid interaction and the initial stresses, possible real movements of the root section, in particular a vertical displacement and a rotation ( $x$  axis).

Fig 18 corresponds to a displacement of 8.9 mm and a  $12^\circ$  rotation. Geometry and initial stresses correspond to 80 mmHg and internal pressure to 120 mmHg.

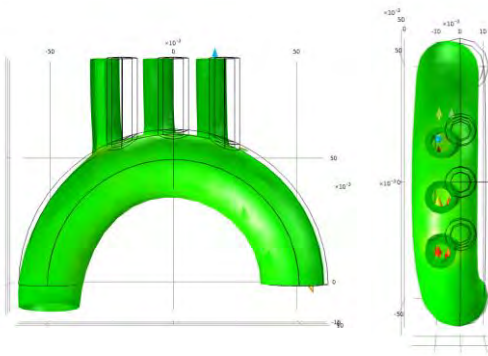


**Figure 16.** Frontal and upper view.

## 5. - Conclusions

A complex fluid solid interaction including initial stresses and root displacements seems possible to be simulated.

This is a preliminary methodology that has been carefully validated in its basic steps, but more results have to be obtained and compared with real data of medical value.

Initial stresses for hyperelastic material have been included, using intensively Comsol and user defined variables.

Some considerations are made to the weak contribution of the boundary load interface of the FSI interface, which seems reasonable to obtain correct results.

## 6. - References

1. J. M. Goicolea Ruigómez, "Biomechanical Factors: Influence on Cardiovascular Function", *Revista Española de Cardiología*, 2005 58:121-5.
2. F.J. Calvo. "Simulación del Flujo Sanguíneo y su Interacción con la Pared Arterial". Tesis doctoral, UPM, Madrid 2006.
3. C. G. Herrera. "Comportamiento Mecánico de la Aorta Ascendente: Caracterización Experimental y Simulación Numérica". Tesis doctoral, UPM, Madrid 2008.
4. Carsten J. Beller, Michel R. Labrosse, et al, "Role of Aortic Root Motion in the Pathogenesis of Aortic Dissection", *Circulation* 2004, 109:763-769.

5. Gianmarc Coppola and Kefu Liu, "Study of compliance Mismatch within a Stented Artery", COMSOL conference 2008 Boston.

6. Ryo Torii, Marie Oshima, et al, "Computer modelling of cardiovascular fluid-structure interactions with the deforming-spatial-domain/stabilized space-time formulation", *CMAME* 195 (2006) 1885-1895.

7. M. A. Esteves, "Modelos computacionales de Interacción Fluido Estructura con Aplicación a la Circulación Sanguínea", Proyecto Fin de Máster, UPV/EHU.2011

## 7. Acknowledgements

This research has been carried out within the framework of the project "Human aorta biomechanics: new models for computations and medical applications" supported by the I+D+I National Plan of the Spanish Ministry of Science and Innovation.